A Review of Mechanisms and Models for Dynamic Strength, Dynamic Failure, and Fragmentation

K.T. Ramesh[a], James D. Hogan[a], Jamie Kimberley[b], Angela Stickle[c], Andrew L. Tonge[a]

[a]*Hopkins Extreme Materials Institute, The Johns Hopkins University, Baltimore, MD 21218*
[b]*New Mexico Institute of Mining and Technology, Socorro, NM 87801*
[c]*Johns Hopkins Applied Physics Laboratory, Laurel, MD 20723*

Abstract

Modeling of catastrophic disruption requires understanding the processes of dynamic failure and fragmentation. This paper summarizes current mechanisms and models for dynamic failure, strength, and fragmentation, reviewing these from a mechanics perspective and with an emphasis on making links to the developing advances in these areas in the engineering and computational mechanics communities. We describe dynamic failure processes, examine size and rate effects, articulate the scaling concepts that arise naturally from these processes, and examine the influences of these processes on effective strength and fragmentation.

Keywords: disruption, strength, failure, dynamic fragmentation, planetary materials, brittle behavior

---

1. Introduction

There is evidence throughout the solar system of catastrophic disruption, particularly as the result of large impacts into asteroids (Williams, 1989; Zappal et al., 1995; Binzel and Xu, 1993; Burbine et al., 2001) and comets (Podolak and Prialnik, 1996; Chapman, 1975). Missions in recent decades (e.g., NEAR, Deep Impact, Hayabusa, Dawn, Rosetta, soon OSIRIS-REx) have revealed new and interesting details about the nature of small bodies in the solar system. Many asteroids have been observed to have impact craters with diameters comparable to the body size (Bottke Jr et al., 2002), suggesting that very large impacts can be below the disruption threshold. In addition, internal structure and damage has been observed on the surface of most small bodies, as is evident

Email addresses: `ramesh@jhu.edu` (K.T. Ramesh), `jd.hogan@jhu.edu` (James D. Hogan), `jamiek@nmt.edu` (Jamie Kimberley), `angela.stickle@jhuapl.edu` (Angela Stickle), `andy.tonge@jhu.edu` (Andrew L. Tonge)

from large-scale fractures observed on Ida: (Sullivan et al., 1996); Eros: (Veverka et al., 2000); and Vesta: (Le Corre et al., 2012; Schenk et al., 2012; Scully et al., 2012). It appears that much of this structure is the consequence of impact-dominated processes.

Our understanding of impact processes is typically limited by two things: first, our understanding of the dynamic material properties and failure processes of the planetary materials that are involved in the impact, and second, our ability to capture these complex processes within computational simulations of these extreme events. Laboratory experiments have been very useful in improving our understanding of impact processes and catastrophic disruption (e.g., Gault (1973); Gault and Wedekind (1969); Fujiwara and Tsukamoto (1980); Nakamura and Fujiwara (1991); Martelli et al. (1994)). Laboratory-scale experiments, however, are orders of magnitude smaller than most of the collisions in the solar system. Thus computational simulations (e.g., Melosh et al. (1992); Benz and Asphaug (1994); Jutzi et al. (2010)) and scaling relationships (Holsapple, 1993; Davis et al., 1994; Housen et al., 1983) have become increasingly critical in understanding large-scale impacts. Hydrocode-based simulations have been shown to be capable of handling many of the complexities of the major impact event, particularly with respect to shockwave propagation and interactions with boundary conditions, and are typically benchmarked against laboratory experiments. Improvements to such simulations and the development of new scaling relationships should result from advances in the understanding and modeling of the failure processes that occur during impact events.

Most of the impact events of interest to planetary science represent extreme dynamic events, which are characterized by the deposition of large amounts of energy in very short times. Because the speeds at which energy can propagate away from the location of deposition are finite (for example, shock speeds), the local energy density rises very rapidly, and so the material seeks new internal pathways to dissipate the energy (for example, fracture, melting, and vaporization). These internal energy pathways are typically referred to as "mechanisms." Which mechanisms are available depends on the materials involved, and which of these mechanisms are exercised depends also on the severity of the impact, and the generalized loading conditions (e.g. impact parameters such as obliquity).

A schematic of the main variables, failure mechanisms and processes in planetary impact events is presented in Figure 1 in terms of the conventional domains associated with a major impact.

Consider an impactor of diameter a impacting a much larger target body at a high velocity V. One characteristic timescale for the event is then given by $\tau_i = a/V$, and the likely phenomena can then be categorized in terms of time after impact, described in terms of multiples of τ_i. This type of domain decomposition can also be performed in terms of length scales using multiples of the impactor diameter. Four domains can be identified, denoted generally as the source, strong shock, strength/flow and structural domains. Within each of these domains, we can identify the expected pressures, strain rates, and temperatures. These variables typically characterize the conditions that are developed in those domains. For example, the domain just under the impactor (called the contact domain) perceives the highest pressures, strain rates and temperatures. For each domain, we also identify critical macroscale processes, the deformation and failure mechanisms, and the kinds of models needed to describe these mechanisms. The material models that are used should be able to account for this range of pressure, strain rate and temperature histories, be able to incorporate these deformation and failure mechanisms in an effective way, and provide the key parameters necessary for the modeling of the critical processes in each domain.

The domains of primary interest to us in this paper are in the shaded region in Figure 1. The materials in this region are under pressures of the order of 10 MPa to 1 GPa, deforming at intermediate strain rates of $10^{-6} - 10^{4}\ s^{-1}$, and undergoing massive failure through the collective behavior of cracks, voids and shear bands. Modeling the response of the material involves the coupling of these damage mechanisms with the rapidly varying stress states associated with the propagating shock, the development of rarefaction fans and subsequent spall from shock release down isentropes, massive fragmentation at intermediate strain rates, fragmentation-induced dilatation ("bulking") and the overall rates of deformation. In practice, few simulation approaches are able to handle all of these phenomena within the same simulation with high fidelity, with particular difficulties often arising from the fragmentation and bulking components.

This paper summarizes current mechanisms and models for dynamic failure, strength, and fragmentation, reviewing these from a mechanics perspective and with an emphasis on making links to the developing advances in these areas in the engineering and computational mechanics communities. Note that the background of the authors is that of experiments and modeling in dynamic mechanics of solids, rather than planetary science, and so it is likely that we cannot adequately represent the extensive literature in this area in planetary science. We therefore do not attempt to capture all of the excellent work already published within the planetary science literature in this area, providing instead representative examples of related work. Finally, we note that reviews such as this are inevitably biased towards the works that are most familiar to the authors, and we apologize in advance to any who feel that their work has been slighted: this is certainly not our intention.

2. Dynamic Failure Mechanics

The specific failure processes that are developed within any given region of the target depend primarily on the material class (e.g. brittle versus ductile) and the current stress state. Figure 2 provides some of the typical failure processes that are developed within each material class as a function of the multiaxial stress state. Note for example, that the influence of confining pressures on failure processes can also be dramatic. Confining stresses can reduce available driving forces for some failure processes like fracture. However, confining stresses can also change the *mode* of failure. For example, Hu et al. (2011) demonstrated that the application of a bi-axial confining stress can re-orient the principal direction of crack growth during compression, producing diffuse shear-dominated failure zones (Figure 3). Some of these mechanisms are not intuitively expected: for example, a homogeneous ductile material subjected to hydrostatic compression generally does not fail, whereas the same ductile material containing inclusions/heterogeneities can develop adiabatic shear bands under hydrostatic compression because the inclusions break symmetry and act as nucleation sites for the failure process. As a consequence, the possibility of large-scale shear localization should be considered in most planetary materials even in regions of nearly hydrostatic compression. Additional details on selected mechanisms in Figure 2 may be found in the following references: necking and void growth (Wu et al., 2003); adiabatic shear bands (Wright, 2002); bifurcation to nucleate voids (Wu et al., 2003); wing cracks (Horii and Nemat-Nasser, 1985); crack shutdown under pressure (Hu et al., 2011); and spallation (Wright and Ramesh, 2009).

The major dynamic failure processes that are developed during large-scale impacts include (but are not limited to):

- Dynamic fracture (nucleation, growth and coalescence of cracks) (Freund, 1998).
- Dynamic void nucleation and growth (leading to spallation) (Meyers, 1994).

- Void collapse (e.g., (Carroll and Holt, 1972; Molinari and Mercier, 2001)). Note that pore compaction can also be a localizing process, e.g. (Issen and Rudnicki, 2000).

- Adiabatic shear banding (dynamic localization of shearing deformations) (Wright, 2002; DORAZIO et al., 2011).

- Amorphization or phase change of some crystal structures (Chen et al., 2003).

Some examples of these failure processes are presented in Figure 4 for a variety of materials (references are noted in the sub-figures). The morphology of the failures is distinct in each case. Since each failure process is typically developed under a particular stress state, the presence of such failures is often used as a signature of the prior existence of that stress state. The associated length scales include the failure size and the failure spacing.

We provide foundational models for each failure mechanism in the next sections. In general, such models typically prescribe five major components: (i) a nucleation criterion; (ii) an onset of growth criterion (sometimes called an initiation criterion), if nucleation has already occurred; (iii) an equation for the growth dynamics; (iv) a description of the interactions with other failures or with boundaries; and (v) a coalescence or runaway instability criterion. The nucleation question is the least well-understood of the five components, and is an active area in multiscale modeling (e.g., Rudd and Belak (2002)). Growth, on the other hand, is relatively well described, although growth dynamics continues to be an area of intense research (e.g., Wilkerson and Ramesh (2014)). In most cases the interaction and coalescence questions are also poorly-understood and are the source of many recent models (e.g., Jacques et al. (2012)).

A consequence of the activation of any of the failure processes presented in Figure 2 are inherent length scales and timescales, which then are manifested in the macroscopic impact event. These scales should ideally be resolved in simulations if the failure process is to be captured, an issue of great importance in engineering because of the need for design of protection systems. However, resolving these scales is often difficult to do from a computational resources viewpoint, particularly for the scales associated with small bodies in the solar system. As an example, the spacing of macroscopic shear bands will be reflected in the fragment sizes (Zhou et al., 2006c), and so the computational scheme must be able to resolve this spacing if fragment sizes are to be predicted. These fragment length scales change with loading path, e.g. when a region of material undergoes hydrostatic compression followed by hydrostatic tension, the initial compressive state may result in shear banding, and the subsequent tensile state is then felt by a damaged material containing shear bands with a spacing that will affect the tensile fragmentation. In this section, we will explore some key failure mechanisms that are activated during catastrophic disruption, and we present some examples of models for these mechanisms. A relatively recent compendium of many of these mechanisms and associated models can be found in the Proceedings of the IUTAM Symposium on Dynamic Fracture and Fragmentation of 2009, with the papers appearing in the International Journal of Fracture in 2010.

An area of particular current growth in the mechanics literature is that of multiscale computational models of failure processes such as shear localization and dynamic fracture. Since these processes *localize* in both space and time, they are intrinsically multiscale. Significant advances in multiscale modeling capabilities are under development, through both sequential (coarse-graining or fine-scaling) and concurrent (hierarchical and partitioned-domain) approaches (a discussion of these is provided by Tadmor and Miller (2012)). Snapshots of the state of the art can now be observed in all of the major mechanics conferences. Much that was considered simply not possible a decade ago is now feasible, e.g. the coupled handling of plasticity and fracture across multiple scales within computational frameworks (Chakravarthy and WA, 2010), and the efficient computational solution of multiscale damage problems (Liu, 2014). An excellent example of these ideas as applied to modeling materials across multiple scales is provided by Phillips (2001), and a more recent discussion of the computational aspects is provided by Fish (2013). Many of these advances are able to bridge across six or more orders of magnitude in length scales, and arose because of the engineering need for microstructure-aware computational mechanics schemes (e.g., Ghosh (2011)) for failure-resistant product design (e.g. jet engines). These theoretical frameworks and computational methods lend themselves also to the much larger scales examined by the planetary science community, although significant challenges remain. Improved models of the disruption and fragmentation of planetary bodies should benefit from such multiscale approaches.

We discuss the major failure mechanisms briefly et seq. The literature on the mechanics of individual failure processes is vast, and so we focus on the key concepts rather than provide a comprehensive review.

2.1. Dynamic fracture

An excellent discussion of fracture mechanics that includes dynamic fracture is presented by Broberg (1999). The elastodynamic solutions corresponding to fast cracks were first presented by Freund, and are summarized in his book on Dynamic Fracture Mechanics (Cambridge University Press). These works generally focus on the propagation of pre-existing cracks. Nucleation of cracks from heterogeneities is a complex problem with solutions that vary widely depending on the nature of the heterogeneity and on the local stress state. A common, if imperfect, approach to nucleation is to define the local maximum tensile stress (say maximum principal stress) σ_{max}, define the heterogeneity size l_h, and then to assume that nucleation occurs when $\sigma_{max} = \alpha \frac{K_{IC}}{\sqrt{2\pi l_h}}$, where K_{IC} is a property (the "fracture toughness") of the matrix material surrounding the heterogeneity and α is a prefactor that is used to identify the "strength" of the heterogeneity (i.e. the pre factor is different for inclusions, pores, and so forth).

For a pre-existing crack of a given length, the onset of tensile crack growth (crack initiation) occurs when the stress intensity factor K_I (which represents the driving force on the crack tip, depends on the stress state and is tabulated for a variety of problems, e.g. Anderson (2004) and the DTD Handbook online) reaches a critical value (the aforementioned fracture toughness): $K_I = K_{IC}$. Fracture toughness data for a number of geological materials is presented by Zhang and Zhao (2014). The stress intensity factor is the variable through which the multiaxial stress state affects the crack tip, and such analyses motivate the development of pressure-dependent behavior of brittle rocks.

Once the crack is growing, the dynamics of crack growth for fast cracks is defined by the rate of change of crack length $\dot{l}$, and is given by

$$\dot{l} = v_c \left(\frac{K_I - K_{IC}}{K_I - K_{IC}/2} \right)^{\beta}, \tag{1}$$

where v_c is the crack speed (an important parameter that must be measured) and β is a parameter that defines the increase in effective crack inertia with crack speed. Crack speeds can vary substantially, but are limited by the Rayleigh wave speed except under pathological conditions (Broberg, 1999). In geomaterials, they are usually of the order of 200-2,000 m/s (Zhang and Zhao, 2014).

Once the cracks are sufficiently large, they will begin to interact (the works of Kachanov (2003) in this area are particularly useful). The general interactions of multiple dynamic cracks are very difficult mechanics problems. Many approaches to describe this interaction have been used, such as assuming a periodic array of cracks (Deng and Nemat-Nasser, 1992; Deshpande et al., 2011), considering self-consistent solutions (Paliwal and Ramesh, 2008), or making structural approximations such as buckling columns (Ashby and Cooksley), 1986). In general, crack interactions result in increased driving force on crack tips, and the crack speed increases (equation 1). Crack interactions are particularly important when estimating the strength of brittle materials.

Eventually the growing cracks will coalesce. Coalescence of cracks is typically only modeled in an approximate manner through either an instability analysis of the ligament between interacting cracks (e.g., Benzerga and Leblond (2010)), through empirical functions that parameterize the instability, or through mode-specific rules (Tang et al. (2001)). Fragmentation follows after coalescence, and so fragment sizes and shapes depend on the full set of nucleation, growth and coalescence behaviors.

Computational modeling of fracture processes is well developed for the growth phase, and there are several commercial and public domain software packages that handle fracture mechanics, including dynamic fracture. These include general purpose commercial finite element packages like Abaqus that include techniques such as cohesive zone modeling, and downloadable software such as FRANC3D developed by academic groups (in this case the Cornell Fracture Group). Such codes are generally capable of tracking crack fronts and crack paths through solids during dynamic failure processes, but the computational cost increases rapidly with increasing numbers of cracks, and convergence with respect to fragmentation remains a major research problem.

2.2. Adiabatic shear localization

Shear localization or shear banding is an instability brought about through the large shearing deformations of materials. Shear bands are of two types: (a) resulting from deformation instabilities associated with evolving parameters in the constitutive equations (Rudnicki and Rice, 1975), and (b) thermal instabilities associated with evolving temperature, adiabatic heating and subsequent thermal softening (Molinari and Clifton, 1987). Deformation instabilities are mathematically easily described in terms of bifurcation analyses, are commonly observed in slow loading problems, and are not discussed further here.

Thermal instabilities lead to a kind of shear band known as an adiabatic shear band (Molinari and Clifton, 1987). These only arise under dynamic loading and are a result of the competition between the timescales associated with the loading dynamics and the timescales associated with the thermal conduction. An excellent summary of the conditions for nucleation of adiabatic shear localization (in terms of the onset of instability) is provided by Wright (2002). Criteria for the onset of adiabatic shear bands typically examine the derivatives of the stress in the stress-strain curve of the material e.g., in terms of strain-hardening, strain-rate-sensitivity and thermal softening of the shear stress, or in terms of the evolution of effective frictional stresses. The canonical works in the area of shear localization and adiabatic shear band development are the books by Wright (2002) and Dodd and Bai (2012).

Once an adiabatic shear band has nucleated, the strain localization evolves in two directions: along the direction of shear (in the form of a shear band tip), and normal to the direction of shear (in the form of the band thickness). Unlike the crack tip, the tip of the shear band is typically poorly defined; however, the propagation of the shear band tip along the direction of shear appears to be similar to that of a shear crack, and so a tip velocity is sometimes identified as equal to a shear crack speed for modeling purposes. A now-classic set of experiments that describes this behavior, with associated analyses, is presented by Zhou et al. (1996). The rate of localization depends strongly on material behavior and the macroscopic stress state (Wright, 2002). For many materials, it is possible to define a finite band thickness that depends on material properties (Dodd and Bai, 2012). The final microstructure within this shear band thickness is typically very different from the initial microstructure of the material, because very large shear strains must be accommodated by the material within the band. An additional mechanism that may be very important in fluid-saturated geophysical materials is that of an effective thermal pressurization produced by the constrained relative thermal expansion of fluids within the band (Platt et al., 2014). Adiabatic shear bands in brittle materials have been recently examined by citeGradySB2011.

The interactions of shear bands define the shear band spacing, and essentially constitute competitions between momentum transport and thermal transport . A detailed analysis of shear band interactions is provided by Zhou et al. (2006c). The shear band spacing may control the apparent fragment size under some conditions, because the shear localization is often the first failure mechanism that is developed during the compressive states that initiate after impact loading, with cracks often following along the shear bands.

From a computational viewpoint, adiabatic shear localization represents a major challenge because of the dynamics involved, the associated length scales, and the evolving local microstructure in the band. The majority of simulations of adiabatic shear localization do not account for the nonlinear evolution of the material behavior within the shear band. Mesh-insensitive computations of shear localization can be obtained by incorporating the thermal conduction length scales in thermo-mechanical simulations, and by incorporating enriched numerical techniques such as XFEM and its relatives. This failure mode remains one of the most challenging dynamic failure mechanisms for simulations.

2.3. *Spall failures under dynamic loading*

There is not, unfortunately, an accessible standard reference on the mechanics of spall failure, but an excellent discussion can be found in the book by Meyers (1994). In the engineering sense used here, spallation is the result of the dynamic nucleation, growth and coalescence of voids or cracks (Meyers, 1994))under a macroscopically hydrostatic tensile state, and are typically observed on the opposite side of the target body from the impact face. The tensile states are generated by the interaction of rarefaction or tension waves coming off free surfaces, and so body geometry plays a big role in the location of spall. Full brittle spall is rare, and so we focus on the ductile (void-driven) spall problem. Void nucleation typically occurs over a very wide range of length scales because of the scales of heterogeneities. For the case of an elastic-plastic solid, it can be rigorously shown that even homogeneous nucleation of voids will occur through a bifurcation process at sufficiently high hydrostatic tensile stresses (Wright and Ramesh, 2009). The presence of a heterogeneity reduces the critical stress that is needed, and thus in general geophysical materials have a distribution of nucleation sites with a corresponding distribution of nucleation stresses. Nucleation can occur at, for example, vacancy clusters (Mori and Meshii, 1964), precipitates (Embury and Nicholson, 1965), inclusions (Thompson and Weihrauch, 1976), large xenoliths and so forth. Most materials of interest to the planetary science community contain pre-existing voids and pores, although the initial porosity will typically be modified by the compressive shocks from the impact.

The classical picture of spall mechanics is the following: voids are nucleated as described above, grow through the development and growth of a plastic zone around the void, and then the interactions of the growing voids leads to the macroscopic spall failure. The "spall strength" is the maximum hydrostatic tensile stress (Antoun et al., 2003) that the material can withstand, is associated with these dynamically growing and interacting voids, and is viewed as a material property (akin to the fracture toughness described earlier). For any given void, the void growth rate is limited by two factors (Wright and Ramesh, 2009): (1) the inertia associated with moving the mass of material away from the current void surface, and (2) the viscoplastic inertia associated with developing plastic flow at sufficiently high rates. The consequence is that the spall strength increases rapidly with the volumetric strain rate (Wright and Ramesh, 2009). The spall strengths of engineering materials are typically measured using plate impact spallation experiments (Meyers, 1994), but there is limited data on the spall strengths of geological materials (e.g., Field (2007)). A first-order and somewhat conservative estimate of the spall strength for effective elastic-plastic solids can be obtained using the analytical procedures described by (Wu et al., 2003). A recent discussion of the theoretical mechanics issues associated with spall (albeit in metals) can be found in Wilkerson and Ramesh (2014).

Spall failures that develop in numerical simulations are typically captured either by explicitly incorporating a spall failure criterion (such as a spall strength) or develop naturally through the evolution of an internal (porosity-type) damage model (such as localization of growing porosity). Validation of computational models of spall is difficult because of the dearth of time-resolved experimental spall data on the materials of interest, and issues of length-scale dominate such computational analyses. An example of the state-of-the-art in time-resolved experimental spall data is provided by the Line VISAR work of Furnish et al. (2009), and demonstrates the statistical nature of the mechanism.

3. Dynamic Failure Mechanics and The Effective Strength of Planetary Materials

The icy, basaltic and chondritic materials that dominate small bodies are generally very heterogeneous, containing multiple constituent phases that may be individually either brittle or ductile. The local behavior may include cracking, shear banding and void growth, while the macroscopic representation of the averaged behavior is usually the "strength," defined as the limiting stress that the material can undergo before measurable permanent deformation, and represented by a limit surface in a six-dimensional stress space (Nemat-Nasser, 2009). The effective strength is a consequence of the local behaviors averaged over some representative volume element or RVE (which scales with mesh/cell size in simulations). The review article by Holsapple (2009) provides an excellent discussion of the strength of planetary materials. In this paper, we focus only on making connections between the underlying failure mechanisms and the effective strength (and later fragmentation).

Generally, a strength model captures (a) the onset of permanent deformation, by defining the yield surface, (b) the amount of incremental plastic deformation that will occur when the stress moves outwards from the yield surface (this is called a flow law) and (c) whether the yield surface itself evolves as a result of deformation (this is called hardening). The evolution of other internal variables (for example, porosity or crack damage) may also need to be defined (Jutzi et al., 2008). The strength model must be defined for all possible loading paths in stress space (e.g. loading in compression, followed by shear, and followed by unloading). Given the variety of possible paths, it is extremely difficult to find validated phenomenological models that describe all of the possible behaviors. This motivates the development of strength models that contain evolving internal variables, where the evolution equation for the internal variable can describe specific physical mechanisms and thus reduce the need for massive suites of experiments for parameter identification. The review article by Holsapple (2009) lists some of the strength models commonly used by the planetary impact community. A model that is used in engineering and that should be considered by the broader community is the Sandia Geomodel (Fossum and Brannon, 2004), which is also efficient and is available in some high-performance codes, and its subsequent development in the form of Kayenta, which provides a generalized framework for complex plasticity models (datasets are available for limestone, tuff and granite). Another model of interest is that developed originally for concrete by de Borst and Gutierrez (1999). The transition from smeared cracks to discrete cracks in a finite element framework has been examined by de Borst et al. (2004). Major challenges remain in obtaining parameters for these models for any given material. A recent substantial data set and review of experimental methods to probe the dynamic strength and failure of geological materials is provided by Zhang and Zhao (2013).

As an alternative to phenomenological models, micromechanics-based models may be used (Paliwal and Ramesh, 2008). These models are based on the underlying deformation mechanisms (such as cracking or twinning) that can be activated in materials subjected to any given loading.

One benefit of these physics-based approaches is that they naturally suggest ways to incorporate strain rate, size scale and variability effects into the strength model. The extension to scales and loading regimes outside of the range of experimental data is a continuing hurdle for problems in planetary and space science. The incorporation of fundamental sub-scale physics through micromechanics-based models provides promise for obtaining more representative outcomes than phenomenological models when simulations are performed in regimes where test data is not available.

Failure mechanisms such as cracking are subscale mechanisms that are averaged over the volume in estimating the effective strength of most geomaterials, and the length scales associated with these mechanisms are such that the effective strength is now a function of sample size. The consequences of the dynamic subscale processes on the strength of planetary materials are threefold. First, the strength of geomaterials is a function of the discretization size, with larger RVEs corresponding to weaker materials. Second, the *variability* in the strength is also a function of the discretization size, with smaller RVEs having greater variability (Graham-Brady, 2010). Third, both the strength and the variability, at any given discretization size, depend on the effective rate of deformation (higher rates lead to higher mean strengths and lower variabilities (Daphalapurkar et al., 2011)). We demonstrate these implications of dynamic failure mechanics for the influence of strain rate, sample size, and sample variability on the effective strength in the next section.

3.1. Defect distributions, failure dynamics and effective strength

A key characteristic of all planetary materials is the kind and degree of heterogeneity (e.g. inclusions and pores), since these typically control the nucleation of failure processes. We refer to these heterogeneities as "defects" in the subsequent discussion. When and how must a defect be considered in the discussion of material behavior? At any given scale, any effective property of a material is determined by volume averaging over RVEs at smaller scales. Thus, for example, pores are averaged to obtain porosity and, therefore, density. However, two materials with the same effective porosity may have very different pore size distributions. Consider one material with a multitude of small pores and one with a few large voids. The failure mechanisms of these two materials may be different because the size of the pores can have a strong impact on the failure process (Katcoff and Graham-Brady, 2014). Thus it may be important to capture not just the average defect density but also the defect distribution in determining effective behavior.

The incorporation of defect distributions and the associated micromechanics can simplify the treatment of disruption problems. The influence of defect-driven nucleation on the failure dynamics introduces a length scale (based on the defect spacing), a nucleation stress scale (based on the defect size), and two time scales: the timescale for the failure to propagate and the timescale for the failures from individual defects to communicate. By comparing these timescales with the timescale associated with the loading dynamics (e.g. the reciprocal of the applied strain rate), we can define different regimes of behavior that guide our development of a material model.

The connections between the defect population and the rate-dependent strength are demonstrated in Figure 5, which considers a brittle solid containing a population of flaws/defects of varying severity (that is, a defect distribution). We move clockwise from the top right quadrant of Figure 5, which shows a probability distribution function $g(s)$ of defect sizes s within the material. These defects are not necessarily internal cracks, but rather heterogeneities in the material that are potential sites for crack nucleation. Fracture mechanics tells us that the stress needed to activate a defect (such as a slit microcrack) decreases as $\frac{1}{\sqrt{s}}$, as shown in the bottom right quadrant of Figure 5. Two different rates of loading, slow and fast, are represented on the bottom left quadrant of Figure 5, which shows the stress as a function of time. At any given time, under slow loading (the red solid line), the most severe (largest) flaw is triggered first, and the growth of the corresponding crack might lead to failure of the structure. Under dynamic loading (the green solid line), while the most severe flaw is still triggered first, the finite-velocity growth of the corresponding crack can be outpaced by the rate of increase of the loading, so that the next-most-severe flaw is triggered before macroscopic failure occurs, and so on. At any given time, the dashed lines show that at low loading rates only the largest defects are activated, while at high loading rates the majority of the defect distribution will be activated. Thus the entire distribution of flaws may be activated in the material under dynamic loading (the concept of higher loading rates initiating the smaller flaws of a distribution is utilized in many studies (Holsapple, 1994a; Melosh et al., 1992).

Full micromechanics calculations (Paliwal and Ramesh, 2008) show that when the crack growth dynamics and self-consistent crack interactions are accounted for, the distribution of activated defects (which is different from the distribution $g(s)$ of available defects) is not necessarily described by the two-parameter Weibull-type function $n = k\varepsilon^m$ (where n is the number of activated defects, ε

is a strain measure and k, m are effective material parameters that must be estimated independent of fracture mechanics). The latter approach using the two-parameter Weibull is used extensively, e.g., (Melosh et al., 1992) and more recently (Huang and Subhash, 2003). The effective strength of the overall material, containing an independently prescribed distribution of defects from which cracks may be activated, can be computed directly from the crack interactions (Paliwal and Ramesh, 2008). This distinction is important in engineering brittle materials, where the defect population is controllable and can be designed, but is generally less useful for rock masses where the initial distribution of defects may not be known a priori.

The modeling frameworks described above allow for crack growth rates that are determined via dynamic fracture mechanics (as opposed to assuming constant crack speeds), determines the population of activated defects using fracture mechanics rather than phenomenology, accounts for self-consistent interactions of cracks and computes effective strength therefrom, and naturally incorporates confinement effects on the dynamics of crack growth and the strength. These concepts lead to an important insight: when it comes to impact loading, bigger is not necessarily weaker. Eventually the effect that bigger bodies are more likely to have bigger defects is outpaced by the effect that bigger bodies take much longer times to break.

The distribution of flaws is commonly characterized using a power law distribution of flaw sizes over many orders of magnitude (Holsapple et al., 2002). The geophysical processes that produce the rock mass typically place an upper bound (s_{max}) on the flaw size in the rock mass, and we assume that the lower bound on the flaw size is s_{min} (in engineered ceramics, entirely different defect distributions are generated by the different processing conditions used to make the material, and the maximum defect size and total defect density are dominated by these processing conditions). Any impact into this rock mass will be modeled using a numerical approach which has some finite spatial resolution. The length scale h introduced by the computational discretization is likely to fall within the limits $s_{min} - s_{max}$ of the flaw size distribution and divides the distribution into “subscale” flaws and “super scale flaws,” the former being smaller than h and the latter being larger than h. Flaws which are larger than h can be resolved explicitly by the computational mesh. The sub scale flaws, smaller than h, cannot be resolved by the computational mesh and therefore must be effectively homogenized and represented using a “strength” model, such as a continuum damage model. The super scale flaws, larger than h, result in failure processes that can be explicitly captured by the simulation, but these failure processes need additional equations (e.g., equations of fracture mechanics) to describe their energetics and their dynamics. Essentially, strength models are used at the subscale while failure models supplement the strength models at larger scales. A variety of techniques have been developed (Pandolfi and Ortiz, 2012; Guy et al., 2012; Moës et al., 2003; Camacho and Ortiz, 1996; Xu and Needleman, 1994) for addressing those flaws which *can* be resolved by the computational method.

Because the strength model used at scales below numerical resolution must average in some sense mechanisms occurring at smaller scales, the strength should generally be anisotropic with evolving anisotropy. As a simple illustration, if a brittle material is first loaded in compression, we should expect that the material will now contain a collection of cracks that are aligned along the principal stress direction (Horii and Nemat-Nasser, 1985). If this sample is now subsequently loaded in tension along the perpendicular direction, the effective strength of the material in that direction will be much lower than the effective strength in the direction of the original compression, so that the strength is now anisotropic. The engineering mechanics community is moving rapidly towards the incorporation of anisotropic strength models in simulations of impact events, but many challenges remain in both formulation and implementation.

3.2. Scaling of rate-dependent strength of geophysical materials

An example of the use of micromechanics to develop a simplified strength model is presented here. A recently developed rate-dependent strength model that incorporates the interaction of a distribution of preexisting flaws and crack growth dynamics has been shown to reasonably describe the dynamic strength of a wide range of brittle solids (Kimberley et al., 2013). By identifying critical time and length scales involved in the problem, a universal relationship between the unconfined compressive strength of a brittle solid, σ_c, and the applied equivalent strain rate, $\dot{\bar{\epsilon}}$, is found:

$$\frac{\sigma_c}{\sigma_0} = 1 + \left(\frac{\dot{\bar{\epsilon}}}{\dot{\epsilon}_0}\right)^{2/3}. \tag{2}$$

Here $\sigma_0 = \alpha \frac{K_{IC}}{\bar{s}\eta^{1/4}}$ and $\dot{\epsilon}_0 = \alpha \frac{c_d}{\bar{s}} \frac{K_{IC}}{E} \eta^{1/4}$ are the characteristic stress and strain rate based on the mechanical (K_{IC} is the fracture toughness, c_d is the dilatational wave speed, E is Young's Modulus), and microstructural properties of the material ($\bar{s}$ is the average flaw size, η is the flaw density). Physical interpretations of these characteristic quantities are given in Kimberley et al. (2013). The

Table 1: Characteristic stress and strain rate parameters for the compressive strength data on the brittle solids presented in Figure 6. Details are presented in (Kimberley et al., 2013)

Material	σ_0 (MPa)	$\dot{\epsilon}_0(s^{-1})$
Limestone (Frew et al., 2001)	70	2.0×10^2
Limestone (Green and Perkins, 1969)	300	5.0×10^3
Basalt (Kumar, 1968)	200	1.0×10^3
MAC 88118 (Kimberley and Ramesh, 2011)	50	2.0×10^2
Concrete (Ross et al., 1995)	53	2.5×10^2

associated parameters are presented in Table 1 (for compression) for some geological materials. The equations describing the characteristic stress and strain rate provide useful tools for examining the effect of material properties and microstructure on the rate dependent strength. This strength scaling captures (Figure 6) the rate-insensitive response of geological materials at low rates as well as the sharp increase in compressive strength observed when these materials are compressed at high rates. Preliminary results show that it can be used to describe tensile failure as well with adjustments to the characteristic stress and strain rate, for reasons discussed in that paper. A similar fracture-based approach to predicting the rate dependent strength was used by Grady and Lipkin (1980) which resulted in a power law dependence of strength with strain rate with an exponent of 1/3. The difference in scaling exponent observed here is a result of the defect distribution and crack interactions. It is also possible to develop scaling exponents for rate-dependence that relate to assumed or measured Weibull distributions of size-dependent strength. In this regard, however, we note that the apparent Weibull modulus of engineering brittle solids is known to be a function of the rate of loading, as discussed by Daphalapurkar et al. (2011).

The associated micromechanics model also demonstrates that the superimposition of confining pressure will result in a linear dependence (Hu et al., 2011) of the deviatoric strength on the pressure (as observed in a number of materials), and suggests that there will be a reduction of the rate dependence of the strength with increasing pressure. The latter prediction has not yet been tested experimentally but is consistent with the success of a number of simulations that use rate-independent strength at high pressures.

3.2.1. Implementation of micromechanics-derived strength models in disruption

Many catastrophic disruption studies define a measure Q^* of the disruption, called the catastrophic disruption threshold and defined as the specific kinetic energy per unit target mass at which the ratio of the mass of the largest fragment to the original target mass becomes 0.5 (Ryan, 2000). Here we present a revised disruption scaling where the results of Kimberley et al. (2013) are incorporated in traditional analytical treatments of catastrophic disruption. In the strength regime, Holsapple (1994b) has shown that

$$Q^* \propto \left(\frac{S}{\rho}\right)^{3\mu/2} U^{(2-3\mu)} \tag{3}$$

where S is a material property with units of stress describing the strength of the target, ρ is the target density, U is the impact velocity and μ is an exponent in the coupling parameter (typically taken to be 0.55 for rocky bodies (Holsapple, 1993)). Making the strength measure in (3) the failure strength described by Kimberley et al. (2013), and approximating the strain rate in the body by $\dot{\epsilon} = U/R$ the following scaling is obtained:

$$Q^* \propto \left(\frac{\sigma_0}{\rho} + \frac{\sigma_0}{\rho}\left(\frac{\dot{\epsilon}}{\dot{\epsilon}_0}\right)^{2/3}\right)^{3\mu/2} U^{(2-3\mu)} \tag{4}$$

The size scaling in the strength regime articulated above has significant shortcomings related to the strength model (e.g. it is developed for uniaxial stress states, and ignores explicit size dependence) and the assumptions related to the disruption process itself (lack of strain rate history, oversimplification of the strain rate distribution in the target body). However, it does provides a view of how micromechanics models may be utilized to evaluate scaling in the strength regime. Ideally the micro mechanical model would be run in a concurrent numerical framework leading to a fully coupled simulation (such simulations are underway, with preliminary results presented by Tonge et al. (2014)). Our current numerical implementations are not efficient enough to allow for full scale simulations of the disruption process, and so we have resorted to incorporating the strength model of Kimberley et al. (2013), which incorporates the key features of the full micromechanics.

Equation (4) is plotted in Figure 7 for an impact velocity of 1 km/s (using a bold black line) together a with summary of earlier scaling laws described by Holsapple et al. (2002). Equation (4) predicts that the strength regime consists of two regions as illustrated in Figure 7. For very small bodies there is a decrease in threshold specific energy with a slope of $-\mu$ in the log-log plot. This corresponds to the high strain rate regime of the strength-rate relationship, and agrees with the experimental measurements on small targets conducted by Housen and Holsapple (1999). As the target size increases the average strain rate in the body decreases and the specific energy needed to disrupt a body reaches a plateau corresponding to the strength observed at low strain rates (as previously noted, crack growth dynamics dominates defect probability at large sizes). This feature is notably absent in all other scaling predictions (other than Durda et al. (1998)), and is a direct result of the strength predicted based on micromechanical approaches. For bodies in the 100m - 10km range this scaling predicts higher catastrophic disruption thresholds as compared to most other predictions in the plot. As the size of the target body increases further, the scaling should of course transition from strength dominated to gravity dominated in which a body may be shattered and reaccumulate, or dispersed.

One possible implication of the disruption threshold presented here is that it would be harder to generate rubble pile bodies from targets in the 1km -10km range. Bodies with higher disruption thresholds are less likely to accumulate after impact because fragments have high enough velocity to escape gravitation of the rest of the fragments. The existence of small rubble pile bodies such as Asteroid 25143 Itokawa could imply that this disruption scaling is simply wrong, or alternatively suggest that Itokawa is the result of reaccumulation of a portion of a larger body that was disrupted. This latter suggestion is supported by observational evidence that suggests that Itokawa is likely the result of fragmentation of a larger parent body (Tsuchiyama et al., 2011).

As can be seen in Figure 7, there is great variation in the strength regime scaling of various authors, all of which adequately agree with the very small scale laboratory observations used to tie the strength scaling to the axes. This highlights the effect that the assumptions regarding strength and failure can have on a predicted scaling outcome. It is our hope that simulations incorporating micromechanical approaches that account for the multiaxial stress states and damage anisotropy will provide new insight into the impact processes shaping our solar system.

4. Dynamic Fragmentation

The rapid deposition of impactor kinetic energy to the interacting bodies during impact results in the initiation of cracks, voids or shear bands from internal defects, and these failure processes then interact and coalesce to form fragments. Under quasi-static loading, fragmentation is dominated by the growth of a few dominant cracks (Rong et al., 1979). Tens of thousands of fragments may still be generated under nominally low-rate conditions (Hogan et al., 2012). Under dynamic loading, many more nucleation sites are activated (Zhou et al., 2006b), resulting in decreasing fragment sizes for increasing strain rates (Grady, 2009b). This fragmentation occurs across many length scales, ranging from the order of the body size down to the micro-scale (e.g., order of minimum defect spacing).

The inherent limits on experimental, numerical and observational resolution results in attention being primarily given to larger scales, but the smaller scales dominate the nucleation problem, and may carry a significant part of the energy at ultra-high strain rates. In experiments, studies are often concerned with quantifying the largest fragment size as, for example, a measure of catastrophic disruption (Fujiwara et al., 1977; Ryan et al., 1991). Measurements of complete distributions are less frequent and characterization of fragments < 1 mm are not widely performed. In simulations, the numerical resolution sets the minimum resolvable fragment size in the absence of a post-processing fragmentation step. For planetary and space science observational data, instrument resolution limitations typically prevent documenting sub-meter fragments on, for example, Itokawa (Fujiwara et al., 2006). Examining these larger fragmentation scales may be sufficient for interpreting some planetary impacts (e.g., Sudbury (Zieg and Marsh, 2005)). Better links between laboratory experiments, numerical simulations, and observational data are needed to bridge these fragmentation length scales. In this section we explore some of these links by examining two important parts of dynamic brittle fragmentation: the average fragment size, and size distributions. A further discussion of many of the topics may be found in the book by Grady (2006), and an additional resource on both ductile and brittle fragmentation is provided by Grady (2009a).

4.1. Fragment size distributions

Statistical and geometric approaches have been pursued to predict fragmentation distributions when experimental results were not available. Lienau (1936) randomly partitioned lines to investigate fragment distributions. Mott and Linfoot (1943) predicted distributions by randomly partitioning geometric shapes with lines. In later work, Grady and Kipp (1985) noted Poisson, binomial, log normal, and Weibull fragmentation distributions can be obtained using similar geometric approaches. Grady (2008) noted that these distribution shapes have a strong dependence on material type, where ductile materials appear to be better characterized with an exponential form and brittle materials follow a power-law shape. Combinations of exponential and power-law functions have also been explored in the literature. The origins of these various forms for the fragment size distribution are presented in the reviews by Åström (2006) and the book chapter by Grady (2009a).

Much interest in brittle fragmentation has been focused on power-law fragment size distributions because of the link to scale-invariance (Turcotte, 1993). Power-law distributions can be modeled as a cascade of breakups (Astrom, 2006) and have the form $N(L) \propto L^{-n}$ where the exponent n is the fractal dimension. In the planetary and space science community, the slopes of power-law distributions is used to constrain collision evolution (Davis et al., 1979; Mazrouei et al., 2014). This fractal dimension ranges between 1.5 to 2.5 for experiments with brittle materials (Hogan et al., 2013a, 2012; Grady, 2009a), 3.1 to 3.5 on Itokawa (Mazrouei et al., 2014), and between 2.2 and 2.7 in catastrophic disruption simulations (Jutzi et al., 2010). Values of approximately 2 may indicate the fragmentation process is mainly surface driven, whereas fractal dimensions closer to 3 suggest the damage is more spatially distributed (Taşdemir, 2009). We emphasize that power-law exponents are strongly related to the measurement or numerical resolution. Grady (2009b) suggested that there exist two governing length scales, λ_e and λ_c, which bound the region of the cumulative distribution described by a power-law function. This idea was explored for dynamic fragmentation of granite by Hogan et al. (2012).

4.2. Characteristic fragment sizes

In addition to computing the fragment size distribution, the prediction of a characteristic length scale, λ, is central to understanding brittle fragmentation events. The prediction of λ enables, for example, fragmentation distributions to be normalized and linked across laboratory experiments and numerical simulations of much larger scales. This characteristic length scale is often taken to be the average or median fragment size. Early works on brittle fragmentation sought to develop relationships between energy input and resulting fragment size (Bond, 1961; Hukki, 1961; von Rittinger, 1876; Kick, 1885; Bergstrom et al., 1961; Bergstrom, 1962; Gilvarry, 1961). Linking energy dissipation with fragmentation was determined to be more robust than geometric arguments, although underlying microstructural effects were not yet considered. In this review, we consider theories developed for predicting rate-dependent average fragment sizes developed by

Grady (2009b), Glenn and Chudnovsky (1986), and Zhou et al. (2006a,b). These are developed for fracture-dominated failure processes. Fragment sizes associated with adiabatic shear band failure follow a different scaling law than that for brittle fracture, as discussed by Zhou et al. (2006c), following on from the work of Wright and Ockendon (1996) and Grady and Kipp (1987).

The average fragment size according to Grady is (Grady, 2009b):

$$L_{Grady} = \left(\frac{48G_c}{\rho\dot{\epsilon}^2}\right)^{1/3} \tag{5}$$

where the fracture energy is related to the square of the fracture toughness K_{IC}. This strain-rate scaling of the average fragment size is used extensively in the community, but, as we will show later, experimental data on the fragmentation of some planetary materials has demonstrated that this approximation strongly overestimates mean fragment sizes at low rates of deformation ($< 10^3\ s^{-1}$) and indeed scales incorrectly with strain rate at these low rates. In contrast, the approach seems to have the correct scaling with strain rate at very high strain rates ($> 10^5\ s^{-1}$). Glenn and Chudnovsky (1986) extended the work by Grady to include the elastic strain energy contribution, which is important at low rates, and predicted a quasi-static average fragment size that is essentially independent of strain rate for low strain rates. They suggested that the average fragment size, L_{GC}, be calculated as:

$$L_{GC} = 4\sqrt{\frac{3}{\alpha}}sinh\left(\frac{\phi}{3}\right) \tag{6}$$

where

$$\phi = sinh^{-1}\left[\beta\left(\frac{3}{\alpha}\right)^{3/2}\right] \tag{7}$$

and $\alpha = \frac{3\sigma_t^2}{\rho E\dot{\epsilon}^2}$, $\beta = \frac{3G_c}{2\rho\dot{\epsilon}^2}$, with E the Young's modulus and σ_t is the tensile strength of the material.

A different approach to predicting average rate-dependent fragmentation sizes uses computational tools that explicitly capture both energetics and dynamics, and that account for the residual damage within fragments as well as the residual kinetic energy associated with wave propagation within fragments. These are process-driven models rather than end-state models. Miller et al. (1999) used cohesive elements in a one-dimensional finite element scheme to investigate brittle fragmentation. These simulations predicted average fragment sizes an order of magnitude smaller than those obtained using the energy-based models. Drugan (2001) accounted for wave interactions for one-dimensional fragmentation of a bar, and predicted average fragment sizes smaller than the Glenn and Chudnovsky (1986) predictions at intermediate rates, while converging with the Grady (2009b) and Glenn and Chudnovsky (1986) models at very high strain rates. This work, as well as the study by Shenoy and Kim (2003) using cohesive elements as simulated defects, established the potential importance of wave interactions during fragmentation of brittle materials. The incorporation of elastic wave propagation and interactions, crack nucleation and growth, as well as defect distributions in a fragmentation simulation was pursued by Zhou et al. (2006a,b) (ZMR) for a much larger range of strain rates than Drugan (2001) and Shenoy and Kim (2003). A range of brittle material properties was examined, and a normalizing strain rate measure was identified. All of the material behaviors were shown to collapse to a single rate-dependent curve for the rate average fragment size. In addition to fragment sizes, Zhou et al. (2006a,b) also derive characteristic time ($t_0 = \frac{EG_c}{\sigma_t^2 c}$), length ($L_0 = ct_0$) and strain rate ($\dot{\epsilon}_0 = \frac{\sigma_t}{Et_0}$) terms used to normalize rate-dependent size predictions, and this resulted in collapsing of size predictions across a wide range of brittle material properties. At low rates, the ZMR model predicts average fragment sizes that are larger than those predicted by Glenn and Chudnovsky (1986) and at higher rates, the ZMR model predicts fragment sizes that are approximately 1/3 to 1/5 the average size predicted by Grady. More sophisticated simulations by Levy and Molinari (2010) extended these computational approaches and included the effect of the initial defect distribution to normalize the average fragment size predictions. Very recent work by Bazant and Caner (2014) provides further advances in understanding of the scaling of fragmentation with respect to strain rate.

4.3. Comparing experiments and fragmentation models

It is nontrivial to compare fragmentation experiments with fragmentation models, because the experimental approaches used to generate fragments almost always result in stress states that are much more complicated than the stress states assumed in the models. For example, most experimental methods associated with impact generate initially compressive stress states that are expected to produce internal failures and this seeds the subsequent fragmentation process. Fragments can be developed from macroscopically compressive states within which very large amounts of strain energy can be stored, and the release of that strain energy can generate very fine fragments. Most experimental methods produce a wide range of strain rates as well, so it can be difficult to decide what strain rate to use for comparison with a model.

Published fragment-size distributions exist, e.g. (Hogan et al., 2013a, 2012) for impact testing. However, the corresponding average fragment sizes were plotted at a strain rate estimated by the ratio of impact velocity to target thickness, without accounting for the difference between compressive and tensile states or the variation in strain rate within the sample. This demonstrates the difficulty of comparison of experiments and models arising from the complexity of the experimental stress and strain rate distributions. Similarly, in their experimental study on the uniaxial compression of SiC-N, Wang and Ramesh (2004) plot their average fragment size against the compressive loading rates. However, the equivalent tensile rate is not equal to the compressive loading rate. In another study, Hogan et al. (2013b) plotted median fragment sizes using a mass-size representation but compared the sizes to a model that used a number-size representation. The lesson here is that there are many sizes and strain rates for which to compare models with, and one should keep this in mind when conclusions are made.

Here we define a specific approach to compare experimental fragmentation results obtained from compression Kolsky bar experiments on basalt (Hogan et al., 2015) with theoretical predictions. Grady and Lipkin (1980) also used Kolsky bar experiments to study the fragmentation of planetary materials. This particular testing technique allows fragmentation distributions to be directly linked with material strength measurements under well-defined stress-state and strain-rate loading conditions, but the comparison of compressive and tensile states must still be made. We choose to define an equivalent tensile problem by converting the strain energy in the compression problem to the kinetic energy in an equivalent expanding ring. A comparison of experimentally measured sizes with models also requires deciding what strain-rates to use for comparison. Here we define an equivalent tensile strain rate ($\dot{\epsilon}_{equi}$), since the models all assume tension. We define the equivalent tensile strain rate by defining an equivalent expanding ring problem with:

$$\dot{\epsilon}_{equi} = \frac{V}{R} \tag{8}$$

where R (m) is the equivalent expanding ring radius and V (m/s) is the velocity of the expansion of the equivalent expanding ring. We can estimate V by assuming that the strain energy in compression is converted to the kinetic energy of an expanding ring. The strain energy (W) in compression is given as:

$$W = \left[\frac{1}{2}\int \bar{\sigma} d\epsilon\right]\nabla = \frac{1}{2}\frac{\sigma t^3}{E} \tag{9}$$

where ϵ is the strain, $\bar{\sigma}$ is the effective stress (Pa), ∇ is the volume (m^3) and t is the specimen size (m) (here we are assuming a cube). In uniaxial compression $\bar{\sigma}$ is equal to the compressive strength. The kinetic energy of an equivalent expanding ring is given as:

$$KE_{ring} = \frac{1}{2}mV_{ring}^2 = \frac{1}{2}\rho(2\pi r)RtV_{ring}^2 = \pi\rho R^2 tV_{ring}^2 \tag{10}$$

where m is the mass (kg). Equating these energies (W=KE) and solving for V_{ring}, we find:

$$V_{ring} = \sqrt{\frac{\bar{\sigma}^2 t^2}{\pi\rho R^2 E}} \tag{11}$$

and correspondingly

$$\dot{\epsilon}_{equi} = \frac{V_{ring}}{R} = \sqrt{\frac{\bar{\sigma}^2 t^2}{\pi\rho R^4 E}} \tag{12}$$

We assume that R is 10x the specimen length. Other radii may be assumed (e.g., 30x specimen length), but our results are relatively insensitive to this change because the applied rate is so low. In the calculation of the model predictions, we use material properties of basalt of ρ=2,870 kg/m^3 (Stickle et al., 2013), E=70 GPa (Stickle et al., 2013) and K_{1c}=1.6 MPa $\sqrt{m}$ (Balme et al., 2004). Following convention, we take σ_t to be 1/10 of the material's quasi-static compressive strength, which is approximately 400 MPa (Stickle et al., 2013).

Shown in Figure 8 are the experimental results from Hogan et al. (2015) and comparisons with the models using the equivalence arguments made above. Note we normalize by the characteristic length (L_0) and strain rates ($\dot{\epsilon}_0$) proposed by Zhou et al. (2006a,b). We see from Figure 8 that current models all over-estimate average fragment sizes. We also point out that the models of Grady (2009b) predict much larger sizes than those of Glenn and Chudnovsky (1986), and Zhou et al. (2006a,b) at these strain rates. In a major planetary impact event, the strain rates produced can be very high over relatively small volumes (close to the source domain in Figure 1), but the rates are much lower over much larger volumes that can participate in the fragmentation process. Thus models such as the Grady-Kipp model may significantly overestimate the fragment sizes over much of the volume. For example, Fig 9A shows the results of computed strain rates from a CTH simulation (Ernst et al., 2009) of a 1km body impacting a half-space at 5km/s, and Fig 9B shows the corresponding strain rate domains in comparison with two fragmentation models. In this case the ZMR model predicts the development of much smaller fragments that are more in line with the large amounts of fines observed near many impact craters. Fig 9B also shows the importance of using updated fragmentation models in the consideration of such events.

Increasingly sophisticated models incorporating, for example, continuum elasticity, inelasticity, and damage mechanics have been developed to capture the behavior of brittle materials (Clayton, 2008; Tonge et al., 2013). However, none of these approaches directly couple fragmentation to the deformation, so that in practice fragment sizes are estimated by stopping the simulation at some ad hoc time, estimating the strain rate distribution, and then using post-processing calculations to extract fragment distributions. This decoupled approach has the major disadvantage of providing solutions that depend on the time chosen to estimate the onset of fragmentation. The inclusions of fracture-inducing heterogeneities (Kraft et al., 2008; Kraft and Molinari, 2008) to naturally account for nucleation, the coupling of fragmentation models to the internal variable theory, and the ability to obtain further fragmentation through granular flow would greatly improve the reliability of such simulations.

5. Summary

This paper summarizes current mechanisms and models for dynamic failure, strength, and fragmentation, reviewing these from a mechanics perspective and with an emphasis on making links to the developing advances in these areas in the engineering and computational mechanics communities. We believe that the effective incorporation of failure processes into large-scale impact simulations through micromechanics-based approaches presents a great opportunity for advancement in the fidelity of simulations of impact and disruption. In this paper, we advocate for a consistent multiscale approach to modeling strength, failure and fragmentation in the context of large-scale numerical simulations, with particular attention paid to the handoff between strength models and failure models in relation to the numerical resolution. When the failure processes are subscale to the computational resolution, the consequence is effective behavior (such as strength) that is anisotropic, size-dependent and rate-dependent. Advances in theoretical descriptions of these behaviors and advances in computational mechanics approaches to multiscale modeling have great promise for producing higher-fidelity simulations of large-scale impact and disruption events.

6. Acknowledgements

This work was supported in part by the NASA Planetary Geology and Geophysics program, and in part by the Hopkins Extreme Materials Institute. KTR acknowledges also the support of the Materials in Extreme Dynamic Environments Collaborative Research Alliance through Cooperative Agreement Number W911NF-12-2-0022.

7. Reference

Anderson, T., 2004. Fracture Mechanics: Fundamentals and Applications. CRC Press.

Antoun, T., Seaman, L., Curran, D., Kanel, G., Razorenov, S., A.V., U., 2003. Spall Fracture (Shock Wave and High Pressure Phenomena). Springer.

Ashby, M., Cooksley), S. H. N., 1986. The failure of brittle solids containing small cracks under compressive stress states. Acta Metallurgica 34 (3), 497 – 510.

Astrom, J. A., 2006. Statistical models of brittle fragmentation. Advances in Physics 55 (3-4), 247–278.

Balme, M., Rocchi, V., Jones, C., Sammonds, P., Meredith, P., Boon, S., 2004. Fracture toughness measurements on igneous rocks using a high-pressure, high-temperature rock fracture mechanics cell. Journal of Volcanology and Geothermal Research 132 (23), 159 – 172, parameterisation and Modelling of Lava Flows.

Bazant, Z., Caner, F., 2014. Impact comminution of solids due to local kinetic energy of high shear strain rate: I. continuum theory and turbulence analogy. Journal of the Mechanics and Physics of Solids 64 (17), 223–235.

Benz, W., Asphaug, E., 1994. Impact simulations with fracture. i. method and tests. Icarus 107 (1), 98–116.

Benzerga, A., Leblond, J.-B., 2010. Ductile fracture by void growth to coalescence. Advances in Applied Mechanics 44, 169–305.

Bergstrom, B., 1962. Energy and size distribution aspects of single particle crushing. In: Proc. 5th Symp. Rock Mechanics. pp. 155–72.

Bergstrom, B., Sollenberger, C., Mitchell Jr, W., 1961. Energy aspects of single particle crushing. Trans. AIME 220, 367–372.

Binzel, R. P., Xu, S., 1993. Chips off of asteroid 4 vesta: Evidence for the parent body of basaltic achondrite meteorites. Science 260 (5105), 186–191.

Bond, F. C., 1961. Crushing and grinding calculations. Allis-Chalmers Manufacturiing Company.

Bottke Jr, W. F., Vokrouhlickỳ, D., Rubincam, D. P., Broz, M., 2002. The effect of yarkovsky thermal forces on the dynamical evolution of asteroids and meteoroids. Asteroids III 395.

Broberg, K., 1999. Cracks and Fracture. Academic Press.

Burbine, T., Buchanan, P., Binzel, R., Bus, S., Hiroi, T., Hinrichs, J., Meibom, A., McCoy, T., 2001. Vesta, vestoids, and the howardite, eucrite, diogenite group: Relationships and the origin of spectral differences. Meteoritics and Planetary Science 36 (6), 761–781.

Camacho, G., Ortiz, M., 1996. Computational modelling of impact damage in brittle materials. International Journal of solids and structures 33 (20), 2899–2938.

Carroll, M., Holt, A., 1972. Static and dynamic pore-collapse relations for ductile porous materials. Journal of Applied Physics 43 (4), 1626–1636.

Chakravarthy, S., WA, C., 2010. Origin of plasticity length-scale effects in fracture. Physical Review Letters 105, 115502.

Chapman, C. R., 1975. The nature of asteroids. Scientific American 232, 24–33.

Chen, M., McCauley, J. W., Hemker, K. J., 2003. Shock-induced localized amorphization in boron carbide. Science 299 (5612), 1563–1566.

Clayton, J. D., 2008. A model for deformation and fragmentation in crushable brittle solids. International Journal of Impact Engineering 35 (5), 269 – 289.

Daphalapurkar, N. P., Ramesh, K. T., Graham-Brady, L., Molinari, J.-F., Feb. 2011. Predicting variability in the dynamic failure strength of brittle materials considering pre-existing flaws. Journal of the Mechanics and Physics of Solids 59 (2), 297–319.

Davis, D., Chapman, C., Greenberg, R., Weidenschilling, S., Harris, A., 1979. Collisional evolution of asteroids-populations, rotations, and velocities. Asteroids 1, 528–557.

Davis, D. R., Ryan, E. V., Farinella, P., 1994. Asteroid collisional evolution: Results from current scaling algorithms. Planetary and Space Science 42 (8), 599–610.

de Borst, R., Gutierrez, M., 1999. Discrete vs smeared crack models for concrete fracture: bridging the gap. International Journal of Fracture 95, 261–277.

de Borst, R., Remmers, J., Needleman, A., Abellan, M., 2004. Discrete vs smeared crack models for concrete fracture: bridging the gap. International Journal for Numerical and Analytical Methods in Geomechanics 28, 583–607.

Deng, H., Nemat-Nasser, S., 1992. Dynamic damage evolution in brittle solids. Mechanics of Materials 14, 83–104.

Deshpande, V. S., Gamble, E., Compton, B. G., McMeeking, R. M., Evans, A. G., Zok, F. W., 2011. A constitutive description of the inelastic response of ceramics. Journal of the American Ceramic Society 94 (s1), s204–s214.

Dodd, B., Bai, Y., 2012. Adiabatic shear localization: frontiers and advances. Elsevier.

DORAZIO, M., FOLCO, L., ZEOLI, A., CORDIER, C., 2011. Gebel kamil: The iron meteorite that formed the kamil crater (egypt). Meteoritics and Planetary Science 46 (8), 1179–1196. URL http://dx.doi.org/10.1111/j.1945-5100.2011.01222.x

Drugan, W., 2001. Dynamic fragmentation of brittle materials: analytical mechanics-based models. Journal of the Mechanics and Physics of Solids 49 (6), 1181 – 1208.

Durda, D. D., Greenberg, R., Jedicke, R., 10 1998. Collisional models and scaling laws: A new interpretation of the shape of the main-belt asteroid size distribution. Icarus 135 (2), 431–440.

Embury, J., Nicholson, R., 1965. The nucleation of precipitates: the system al-zn-mg. Acta Metallurgica 13 (4), 403–417.

Ernst, C. M., Barnouin-Jha, O. S., Ramesh, K. T., Swaminathan, P. K., Kimberley, J., 2009. Strain rate and dynamic fracturing in planetary-scale impacts. In: Lunar and Planetary Institute Science Conference Abstracts. Vol. 40.

Field, J., 2007. Spall strength of geomaterials. In: Shock Compression of Condensed Matter.

Fish, J., 2013. Practical Multiscaling. Wiley.

Fossum, A. F., Brannon, R. M., 2004. The sandia geomodel: theory and users guide.

Freund, L., 1998. Dynamic Fracture Mechanics. Cambridge University Press.

Frew, D. J., Forrestal, M. J., Chen, W., Mar 2001. A split hopkinson pressure bar technique to determine compressive stress-strain data for rock materials. Experimental Mechanics 41 (1), 40–46.

Fujiwara, A., Kamimoto, G., Tsukamoto, A., 1977. Destruction of basaltic bodies by high-velocity impact. Icarus 31 (2), 277 – 288.

Fujiwara, A., Kawaguchi, J., Yeomans, D., Abe, M., Mukai, T., Okada, T., Saito, J., Yano, H., Yoshikawa, M., Scheeres, D., et al., 2006. The rubble-pile asteroid itokawa as observed by hayabusa. Science 312 (5778), 1330–1334.

Fujiwara, A., Tsukamoto, A., 1980. Experimental study on the velocity of fragments in collisional breakup. Icarus 44 (1), 142 – 153.

Furnish, M., Chhabildas, L., Reinhart, W., Trott, W., Vogler, T., 2009. Determination and interpretation of statistics of spatially resolved waveforms in spalled tantalum from 7 to 13 gpa. International Journal of Plasticity 25, 587–602.

Gault, D., 1973. Displaced mass, depth, diameter, and effects of oblique trajectories for impact craters formed in dense crystalline rocks. The moon 6 (1-2), 32–44.

Gault, D., Wedekind, J., 1969. The destruction of tektites by micrometeoroid impact. J. Geophys. Res. 74 (27), 6780–6794, cited By (since 1996)30.

Ghosh, S., 2011. Multiscale Characterization and Domain Partitioning for Multiscale Analysis of Heterogeneous Materials. Springer.

Gilvarry, J., 1961. Fracture of brittle solids. i. distribution function for fragment size in single fracture (theoretical). Journal of Applied Physics 32 (3), 391–399.

Glenn, L. A., Chudnovsky, A., Feb. 1986. Strain and energy effects on dynamic fragmentation. Journal of Applied Physics 59 (4), 1379 –1380.

Grady, D., 2009a. Dynamic fragmentation of solids. In: Shock Wave Science and Technology Reference Library, Vol. 3. Springer Berlin Heidelberg, pp. 1–108.

Grady, D., Kipp, M., 1985. Geometric statistics and dynamic fragmentation. Journal of Applied Physics 58 (3), 1210–1222.

Grady, D., Kipp, M., 1987. The growth of unstable thermoplastic shear with application to steady-wave shock compression in solids. Journal of the Mechanics and Physics of Solids 35, 95119.

Grady, D. E., 2006. Fragmentation of rings and shells: the legacy of N.F. Mott. Springer.

Grady, D. E., 2008. Fragment size distributions from the dynamic fragmentation of brittle solids. International Journal of Impact Engineering 35 (12), 1557 – 1562, hypervelocity Impact Proceedings of the 2007 Symposium - HVIS 2007.

Grady, D. E., 2009b. Length scales and size distributions in dynamic fragmentation. International Journal of Fracture 163 (1–2), 85–99.

Grady, D. E., Lipkin, J., 1980. Criteria for impulsive rock fracture. Geophysical Research Letters 7 (4), 255–258.

Graham-Brady, L., 2010. Statistical characterization of meso-scale uniaxial compressive strength in brittle materials with randomly occurring flaws. International Journal of Solids and Structures 47 (18-19), 2398–2413.

Green, S. J., Perkins, R. D., 1969. Uniaxial compression tests at strain rates from 0.0001/sec. to 1000/sec. on three geologic materials. Technical Report MSL-68-6, General Motors Technical Center Warren Mich Materials and Structures Lab, United States.

Guy, N., Seyedi, D. M., Hild, F., 2012. A probabilistic nonlocal model for crack initiation and propagation in heterogeneous brittle materials. International Journal for Numerical Methods in Engineering 90 (8), 1053–1072.

Hogan, J., Plescia, J., El Mir, C., Ramesh, K., Apr. 2015. Dynamic brittle fragmentation: Probing the byproducts of hypervelocity impact in space. In: 2015 Hypervelocity Impact Symposium (HVIS 2015). Boulder, USA.

Hogan, J. D., Castillo, J. A., Rawle, A., Spray, J. G., Rogers, R. J., 2013a. Automated microscopy and particle size analysis of dynamic fragmentation in natural ceramics. Engineering Fracture Mechanics 98 (0), 80 – 91.

Hogan, J. D., Rogers, R. J., Spray, J. G., Boonsue, S., 2012. Dynamic fragmentation of granite for impact energies of 6 to 28 j. Engineering Fracture Mechanics 79 (0), 103 – 125.

Hogan, J. D., Spray, J. G., Rogers, R. J., Vincent, G., Schneider, M., 2013b. Dynamic fragmentation of planetary materials: Ejecta length quantification and semi-analytical modelling. International Journal of Impact Engineering 62 (0), 219 – 228.

Holsapple, K., 1993. The scaling of impact processes in planetary sciences. Annual Review of Earth and Planetary Sciences 21, 333–373.

Holsapple, K., Dec. 1994a. Catastrophic disruptions and cratering of solar-system bodies - a review and new results. Planetary and Space Science 42 (12), 1067–1078.

Holsapple, K., 1994b. Catastrophic disruptions and cratering of solar system bodies: A review and new results. Planetary and Space Science 42 (12), 1067–1078.

Holsapple, K., Giblin, I., Housen, K., Nakamura, A., Ryan, E., 2002. Asteroid impacts: Laboratory experiments and scaling laws. Asteroids III 1, 443–462.

Holsapple, K. A., 2 2009. On the ”strength” of the small bodies of the solar system: A review of strength theories and their implementation for analyses of impact disruptions. Planetary and Space Science 57 (2), 127–141.

Horii, H., Nemat-Nasser, S., 1985. Compression-induced microcrack growth in brittle solids: Axial splitting and shear failure. Journal of Geophysical Research: Solid Earth (1978–2012) 90 (B4), 3105–3125.

Housen, K., Schmidt, R., Holsapple, K., 1983. Crater ejecta scaling laws: Fundamental forms based on dimensional analysis. Journal of Geophysical Research: Solid Earth (1978–2012) 88 (B3), 2485–2499.

Housen, K. R., Holsapple, K. A., 1999. Scale effects in strength-dominated collisions of rocky asteroids. Icarus 142 (1), 21 – 33.

Hu, G., Ramesh, K., Cao, B., McCauley, J., 2011. The compressive failure of aluminum nitride considered as a model advanced ceramic. Journal of the Mechanics and Physics of Solids 59 (5), 1076–1093.

Huang, C., Subhash, G., 2003. Influence of lateral confinement on dynamic damage evolution during uniaxial compressive response of brittle solids. Journal of the Mechanics and Physics of Solids 51, 1089–1105.

Hukki, R., 1961. Proposal for a solomonic settlement between the theories of von rittinger, kick, and bond. Trans. AIME 220, 403–408.

Issen, K., Rudnicki, J., 2000. Conditions for compaction bands in porous rock. Journal of Geophysical Research 105, 21529–21536.

Jacques, N., Mercier, S., Molinari, A., 2012. Void coalescence in a porous solid under dynamic loading conditions. International Journal of Fracture 173, 203–213.

Jutzi, M., Benz, W., Michel, P., 2008. Numerical simulations of impacts involving porous bodies: I. implementing sub-resolution porosity in a 3d sph hydrocode. Icarus 198 (1), 242–255.

Jutzi, M., Michel, P., Benz, W., Richardson, D. C., 2010. Fragment properties at the catastrophic disruption threshold: The effect of the parent bodys internal structure. Icarus 207 (1), 54 – 65.

Kachanov, M., 2003. On the problems of crack interactions and crack coalescence. International Journal of Fracture 120, 537–543.

Katcoff, C., Graham-Brady, L., 2014. Modeling dynamic brittle behavior of materials with circular flaws or pores. International Journal of Solids and Structures 51 (3), 754–766.

Kick, F., 1885. Das Gesetz der proportionalen Widerstände und seine Anwendungen. Felix.

Kimberley, J., Ramesh, K., Daphalapurkar, N., 2013. A scaling law for the dynamic strength of brittle solids. Acta Materialia 61 (9), 3509 – 3521.

Kimberley, J., Ramesh, K. T., 2011. The dynamic strength of an ordinary chondrite. Meteoritics and Planetary Science 46 (11), 1653–1669.

Kraft, R., Molinari, J., 2008. A statistical investigation of the effects of grain boundary properties on transgranular fracture. Acta Materialia 56 (17), 4739 – 4749.

Kraft, R., Molinari, J., Ramesh, K., Warner, D., 2008. Computational micromechanics of dynamic compressive loading of a brittle polycrystalline material using a distribution of grain boundary properties. Journal of the Mechanics and Physics of Solids 56 (8), 2618 – 2641.

Kumar, A., 06 1968. The effect of stress rate and temperature on the strength of basalt and granite. Geophysics 33 (3), 501–510.

Le Corre, L., Reddy, V., Becker, K., O'Brien, D., Palmer, E., Li, J., Gaskell, R., Denevi, B., Nathues, A., Sierks, H., et al., 2012. Nature of orange ejecta around oppia and octavia craters on vesta from dawn framing camera. In: AAS/Division for Planetary Sciences Meeting Abstracts. Vol. 44.

Levy, S., Molinari, J., 2010. Dynamic fragmentation of ceramics, signature of defects and scaling of fragment sizes. Journal of the Mechanics and Physics of Solids 58 (1), 12 – 26.

Lienau, C., 1936. Random fracture of a brittle solid. Journal of the Franklin Institute 221 (4), 485 – 494.

Liu, Y. e. a., 2014. A regularized phenomenological multiscale damage model. INTERNATIONAL JOURNAL FOR NUMERICAL METHODS IN ENGINEERING 99, 867–887.

Martelli, G., Ryan, E., Nakamura, A., Giblin, I., 1994. Catastrophic disruption experiments: Recent results. Planetary and Space Science 42 (12), 1013–1026.

Mazrouei, S., Daly, M., Barnouin, O., Ernst, C., DeSouza, I., 2014. Block distributions on itokawa. Icarus 229, 181–189.

Melosh, H., Ryan, E., Asphaug, E., 1992. Dynamic fragmentation in impacts: Hydrocode simulation of laboratory impacts. Journal of Geophysical Research: Planets (1991–2012) 97 (E9), 14735–14759.

Meyers, M., 1994. Dynamic Behavior of Materials. Wiley Interscience.

Miller, O., Freund, L., Needleman, A., 1999. Modeling and simulation of dynamic fragmentation in brittle materials. International Journal of Fracture 96 (2), 101–125.

Moës, N., Cloirec, M., Cartraud, P., Remacle, J.-F., 2003. A computational approach to handle complex microstructure geometries. Computer methods in applied mechanics and engineering 192 (28), 3163–3177.

Molinari, A., Clifton, R., 1987. Analytical characterization of shear localization in thermoviscoplastic materials. Journal of Applied Mechanics 54, 806–812.

Molinari, A., Mercier, S., 2001. Micromechanical modelling of porous materials under dynamic loading. Journal of the Mechanics and Physics of Solids 49, 1497–1516.

Mori, T., Meshii, M., 1964. On the nucleation of vacancy clusters in gold. Acta metallurgica 12 (1), 104–106.

Mott, N. F., Linfoot, E. H., February 1943. A theory of fragmentation. Tech. Rep. vol. AC3348, United Kingdom Ministry of Supply, UK.

Nakamura, A., Fujiwara, A., 1991. Velocity distribution of fragments formed in a simulated collisional disruption. Icarus 92 (1), 132–146.

Nemat-Nasser, S., 2009. Plasticity: A Treatise on Finite Deformation of Heterogeneous Inelastic Materials. Cambridge University Press.

Paliwal, B., Ramesh, K., 2008. An interacting micro-crack damage model for failure of brittle materials under compression. Journal of the Mechanics and Physics of Solids 56 (3), 896–923.

Pandolfi, A., Ortiz, M., 2012. An eigenerosion approach to brittle fracture. International Journal for Numerical Methods in Engineering 92 (8), 694–714.

Phillips, R., 2001. Crystals, Defects and Microstructures: Modeling Across Scales. Cambridge University Press.

Platt, J., Rudnicki, J., Rice, J., 2014. Stability and localization of rapid shear in fluid-saturated fault gouge: 2. localized zone width and strength evolution. Journal of Geophysical Research Solid Earth 119, 43344359.

Podolak, M., Prialnik, D., 1996. Models of the structure and evolution of comet p/wirtanen. Planetary and Space Science 44 (7), 655 – 664.

Rong, C., Xiao-Xin, Y., Hung-Sen, X., 1979. Studies of the fracture of gabbro. International Journal of Rock Mechanics and Mining Sciences and Geomechanics Abstracts 16 (3), 187 – 193.

Ross, C., Tedesco, J., Kuennen, S., 1995. Effects of strain rate on concrete strength. ACI Materials Journal 92 (1).

Rudd, R., Belak, J., 2002. Void nucleation and associated plasticity in dynamic fracture of polycrystalline copper: an atomistic simulation. Computational Materials Science 24, 148–153.

Rudnicki, J., Rice, J., 1975. Conditions for the localization of deformation in pressure-sensitive dilatant materials. Journal of Mechanics and Physics of Solids 23, 371–394.

Ryan, E. V., 2000. Asteroid fragmentation and evolution of asteroids. Annual Review of Earth and Planetary Sciences 28 (1), 367–389.

Ryan, E. V., Hartmann, W. K., Davis, D. R., 1991. Impact experiments 3: Catastrophic fragmentation of aggregate targets and relation to asteroids. Icarus 94 (2), 283 – 298.

Schenk, P., OBrien, D. P., Marchi, S., Gaskell, R., Preusker, F., Roatsch, T., Jaumann, R., Buczkowski, D., McCord, T., McSween, H. Y., et al., 2012. The geologically recent giant impact basins at vestas south pole. Science 336 (6082), 694–697.

Scully, J., Russell, C., Yin, A., Williams, D., Blewett, D., Buczkowski, D., Ammannito, E., Roatsch, T., Preusker, F., Le Corre, L., et al., 2012. Geologic mapping of the av-4 domitia quadrangle of asteroid 4 vesta. In: EGU General Assembly Conference Abstracts. Vol. 14. p. 3251.

Shenoy, V., Kim, K.-S., 2003. Disorder effects in dynamic fragmentation of brittle materials. Journal of the Mechanics and Physics of Solids 51 (1112), 2023 – 2035.

Stickle, A., Kimberley, J., Ramesh, K., 2013. Dynamic strength experiments on basalt with applications to cratering on mercury. In: Lunar and Planetary Institute Science Conference Abstracts. Vol. 44. p. 3021.

Sullivan, R., Greeley, R., Pappalardo, R., Asphaug, E., Moore, J., Morrison, D., Belton, M., Carr, M., Chapman, C., Geissler, P., Greenberg, R., Granahan, J., III, J. H., Kirk, R., McEwen, A., Lee, P., Thomas, P., Veverka, J., 1996. Geology of 243 ida. Icarus 120 (1), 119 – 139.

Tadmor, R., Miller, R., 2012. Modeling Materials: Continuum, Atomistic and Multiscale Techniques. Cambridge University Press.

Tang, C., Lina, P., Wong, R., Chau, K., 2001. Analysis of crack coalescence in rock-like materials containing three flaws, part ii: numerical approach. International Journal of Rock Mechanics & Mining Sciences 38, 925–939.

Taşdemir, A., 2009. Fractal evaluation of particle size distributions of chromites in different comminution environments. Minerals Engineering 22 (2), 156–167.

Thompson, A. W., Weihrauch, P. F., 1976. Ductile fracture: nucleation at inclusions. Scripta Metallurgica 10 (2), 205–210.

Tonge, A., Ramesh, K., Barnouin, O., 2014. Large impacts on airless bodies: The himeros event on eros. In: Lunar and Planetary Institute Science Conference Abstracts. Vol. 45. p. 1998.

Tonge, A. L., Kimberley, J., Ramesh, K., 2013. A consistent scaling framework for simulating high rate brittle failure problems. Procedia Engineering 58 (0), 692 – 701.

Tsuchiyama, A., Uesugi, M., Matsushima, T., Michikami, T., Kadono, T., Nakamura, T., Uesugi, K., Nakano, T., Sandford, S. A., Noguchi, R., et al., 2011. Three-dimensional structure of hayabusa samples: origin and evolution of itokawa regolith. Science 333 (6046), 1125–1128.

Turcotte, D. L., 1993. Fractals and chaos in geology and geophysics. Cambridge University Press, United Kingdom.

Veverka, J., Robinson, M., Thomas, P., Murchie, S., Bell, J., Izenberg, N., Chapman, C., Harch, A., Bell, M., Carcich, B., et al., 2000. Near at eros: Imaging and spectral results. Science 289 (5487), 2088–2097.

von Rittinger, R., 1876. Textbook of mineral dressing. Ernst and Korn.

Wang, H., Ramesh, K., 2004. Dynamic strength and fragmentation of hot-pressed silicon carbide under uniaxial compression. Acta Materialia 52 (2), 355 – 367.

Wilkerson, J., Ramesh, K., 2014. A dynamic void growth model governed by dislocation kinetics. Journal of the Mechanics and Physics of Solids 70, 262–280.

Williams, J., 1989. In: R. P. Binzel, T. G., Matthews, M. S. (Eds.), Asteroid family identification and proper elements. In Asteroids II. Univ. of Arizona Press, Tucson, p. 10341072.

Wright, T., 2002. The physics and mathematics of adiabatic shear bands. Cambridge University Press.

Wright, T., Ockendon, H., 1996. A scaling law for the effect of inertia on the formation of adiabatic shear bands. International Journal of Plasticity 12, 927–934.

Wright, T., Ramesh, K., 2009. Statistically informed dynamics of void growth in rate dependent materials. International Journal of Impact Engineering 36 (10), 1242 – 1249.

Wu, X., Wright, T., Ramesh, K., 2003. The effects of thermal softening and heat conduction on the dynamic growth of voids. International Journal of Solids and Structures 40 (17), 4461 – 4478.

Xu, X.-P., Needleman, A., 1994. Numerical simulations of fast crack growth in brittle solids. Journal of the Mechanics and Physics of Solids 42 (9), 1397–1434.

Zappal, V., Bendjoya, P., Cellino, A., Farinella, P., Froeschl, C., 1995. Asteroid families: Search of a 12,487-asteroid sample using two different clustering techniques. Icarus 116 (2), 291 – 314.

Zhang, Q., Zhao, J., 2013. A review of dynamic experimental techniques and mechanical behaviour of rock materials. Rock Mechanics and Rock Engineering, 1–68.

Zhang, Q., Zhao, J., 2014. Quasi-static and dynamic fracture behaviour of rock materials: phenomena and mechanisms. International Journal of Fracture 189, 1–32.

Zhou, F., Molinari, J. F., Ramesh, K., 2006a. Analysis of the brittle fragmentation of an expanding ring. Computational Materials Science 37 (1-2), 74 – 85.

Zhou, F., Molinari, J. F., Ramesh, K. T., 2006b. Effects of material properties on the fragmentation of brittle materials. International Journal of Fracture 139, 169–196.

Zhou, F., Wright, T., Ramesh, K., 2006c. The formation of multiple adiabatic shear bands. Journal of the Mechanics and Physics of Solids 54 (7), 1376 – 1400.

Zhou, M., Rosakis, A., Ravichandran, G., 1996. Dynamically propagating shear bands in impact-loaded prenotched plates-i. experimental investigations of temperature signatures and propagation speed. Journal of Mechanics and Physics of Solids 44, 981–1006.

Zieg, M. J., Marsh, B. D., 2005. The sudbury igneous complex: Viscous emulsion differentiation of a superheated impact melt sheet. Geological Society of America Bulletin 117 (11-12), 1427–1450.

List of Tables

List of Figures

Domain	Source	Shock	Strength/Flow	Structure/ Interior
Pressure, Pa	10^{11}	10^{9}	10^{7}	10^{6}-10^{7}
Strain Rate, s	10^{5}	10^{2}-10^{4}	10^{-2}-10^{1}	10^{-6}
Temperature, K	10^{3}-10^{4}	10^{2}	10^{2}	10^{1}-10^{2}
Critical Processes	Strong Shocks, Jetting	Propagating shocks, excavation flow	Collapse mechanisms, post-shock strength	Interactions of cracks and waves with internal structure
Failure Mechanisms	Melting, Vaporization, Phase Transitions	Massive cracking Massive shear banding Massive void growth	Shear zones Collapsed bands Comminuted flow	Cracking
Kinds of Models	Equation of State	Plasticity Dynamic fracture, shear localization, spallation	Fragmentation, plasticity, granular flow	Structural deformation and failure

Fig. 1: Schematic of mechanistic domains and associated mechanisms in catastrophic disruption and asteroid impact. Note that $\tau_i \sim \frac{a}{V}$ is an impactor-dependent timescale.

	Uniaxial Tension	Uniaxial Compression	Hydrostatic Compression	Hydrostatic Tension	Shear	Geologic Material Example
Homogeneous Ductile Material	Necking, void growth	Adiabatic shear bands	None	Bifurcation to nucleate voids	Adiabatic shear bands	Deep heated rocks, planetary cores, iron meteorites
Homogeneous Brittle	Bifurcation to nucleate cracks	None	None	Bifurcation to nucleate cracks	Amorphization?	Bedrock (e.g., lava flows); some minerals
Brittle and Cracked	Tensile fracture	Wing cracks	Shutdown cracks, shear bands	Brittle Spallation	Mixed Mode fracture	Bedrock; sedimentary rocks; megaregolith
Brittle and Porous	Tensile fracture	Wing cracks	Shear bands, microbuckling, kink bands	Spallation	Shear cracks	Sedimentary rocks; regolith; fractured bedrock; ice; asteroids
Brittle with Inclusions	Tensile fracture	Wing cracks	Shear bands	Spallation	Shear cracks	Chondrites, Asteroids
Ductile with Inclusions	Void nucleation	Void nucleation	None	Spallation	Shear bands	Lava flows
Ductile and Porous	Necking, void growth	Compaction, microbuckling	Compaction, microbuckling	Spallation	Void shear mechanisms	Metallic meteorites?

Fig. 2: Failure processes that may be developed during various stress states within dynamic loading. Each region of the target body goes through a complex history of multiaxial stress states and deformation states during a catastrophic disruption event. The typical failure processes that are developed under example stress states are shown. Note that the strength of a material element will also be affected by the failure processes developed over the stress path.

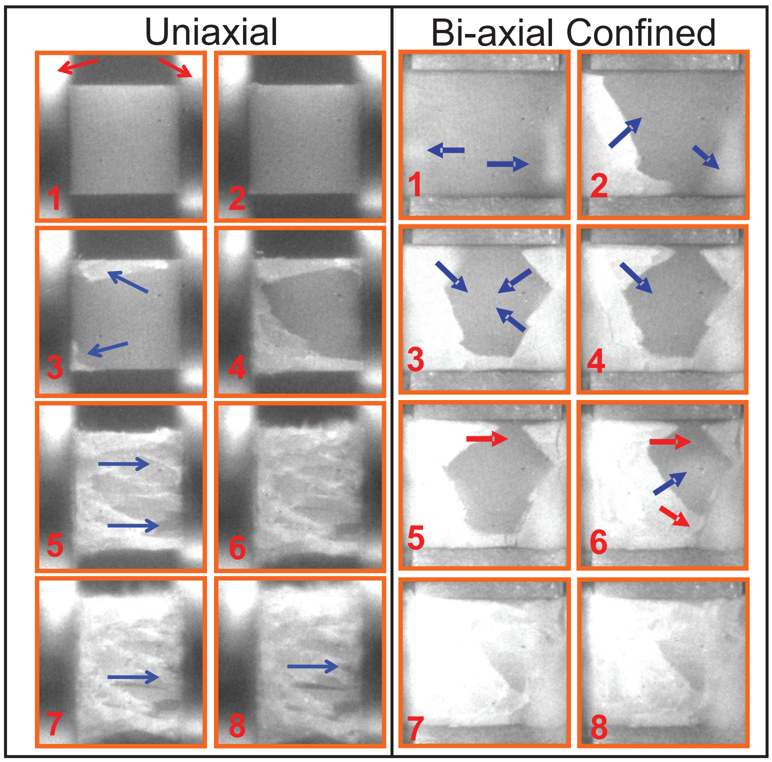

Fig. 3: Influence of confinement on failure process in brittle solids (aluminum nitride in this case) (Hu et al., 2011). Photographs taken every 2 microseconds with exposure times of 500 nanoseconds. (a) Unconfined uniaxial dynamic compressive loading in the horizontal direction. (b) Failure during planar confinement (in the vertical direction) and dynamic compressive loading (in the horizontal direction). Note the development of axial cracks, propagating at speeds of several hundred m/s in (a), but none of these are observed in (b).

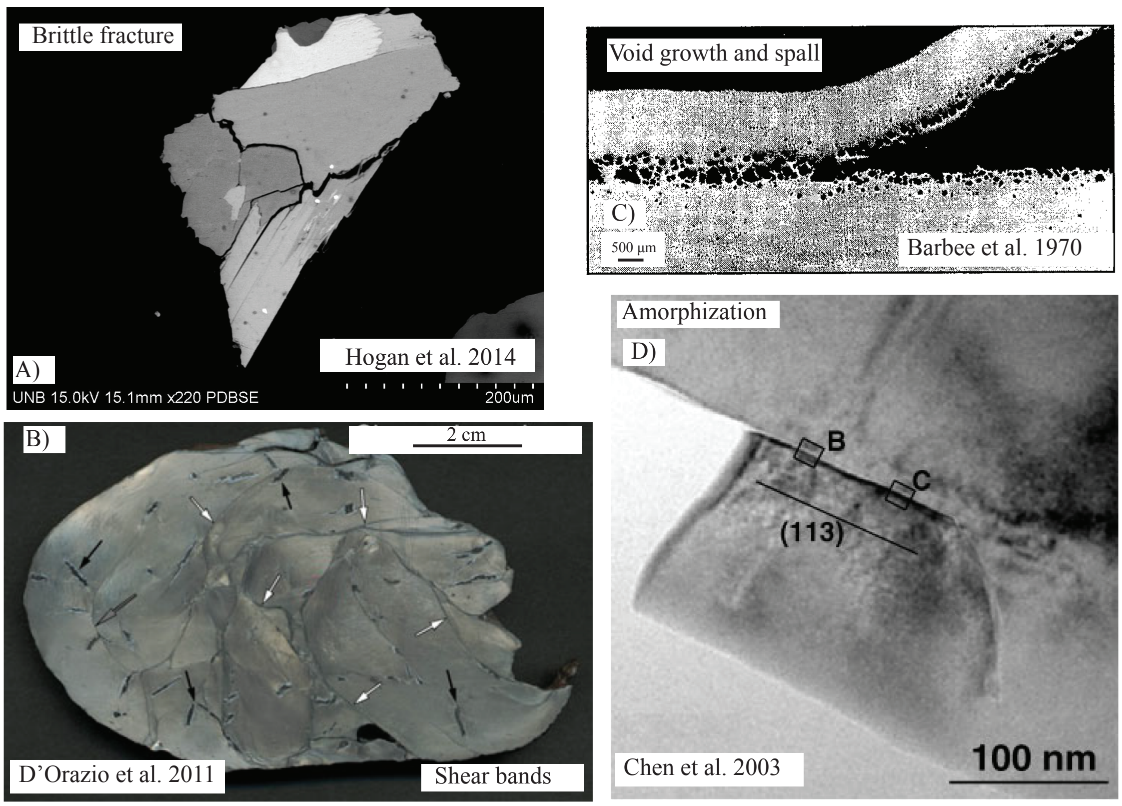

Fig. 4: Examples of failure processes: (a) brittle fracture, (b) shear bands, (c) void growth and spallation, and (d) amorphization. Note that a variety of length scales are represented in this figure, and all of these processes can lead to fragmentation.

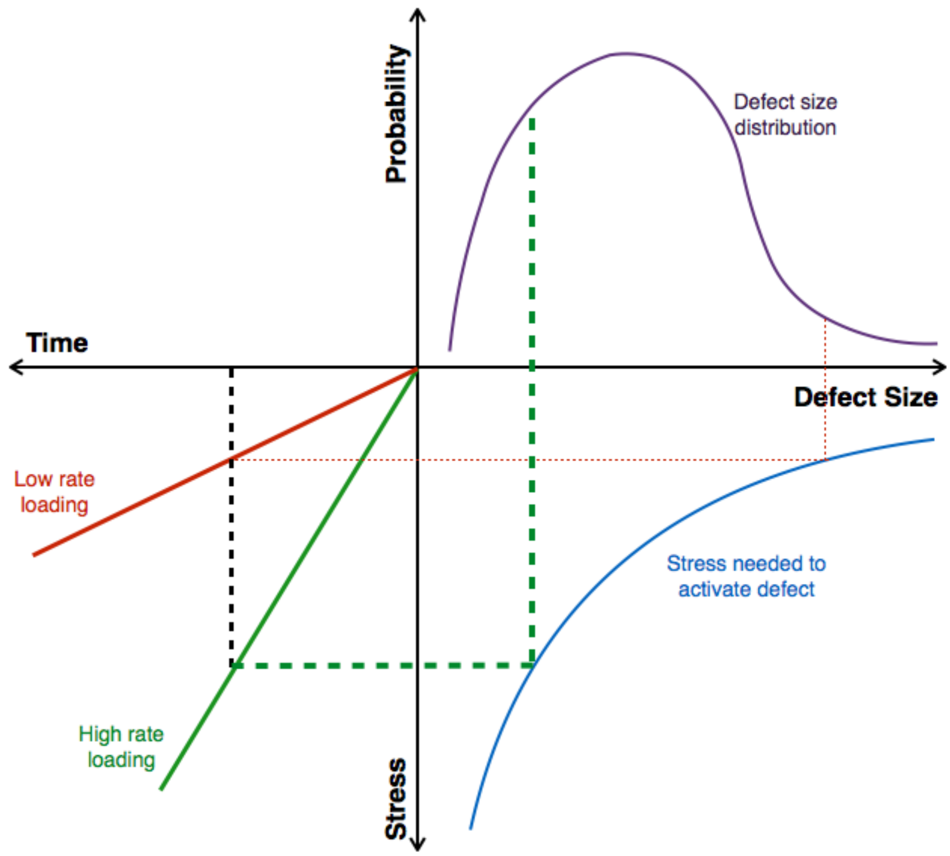

Fig. 5: Multipart schematic showing the influence of rate of loading on the activation of defects in a material containing a distribution of defects. The probability of finding a defect of size s is shown in the top right quadrant. The bottom right quadrant shows how the activation stress depends on the defect size. The bottom left quadrant shows how the applied stress might vary with time, with the red solid line showing a low loading rate and the green solid line showing a high loading rate. At any given time, the dashed lines show that at low loading rates only the largest defects are activated, while at high loading rates the majority of the defect distribution will be activated.

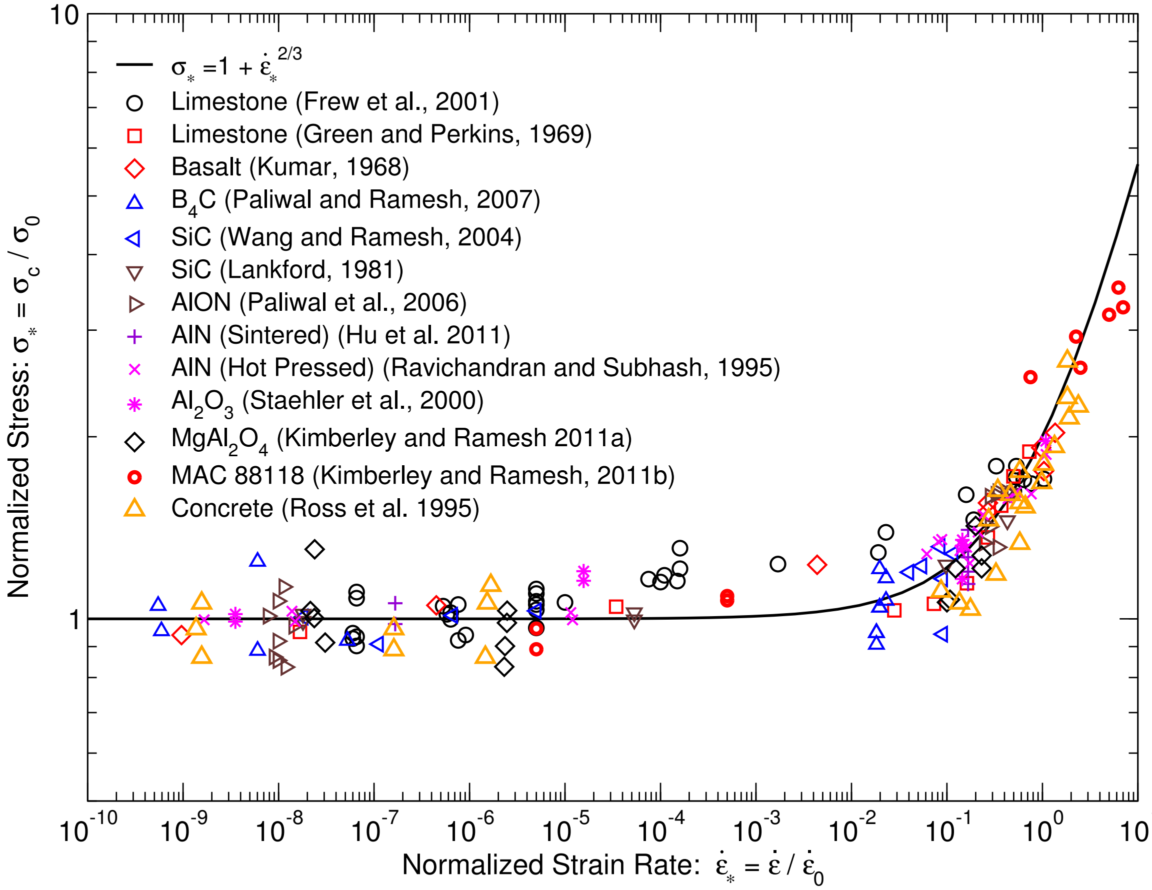

Fig. 6: All brittle solids, including geophysical and engineering materials, appear to follow a universal dependence of the (a) compressive and (b) tensile strengths on the strain rate (Kimberley et al., 2013). This results from the KRD scaling analysis of the influence of a defect distribution on fracture dynamics.

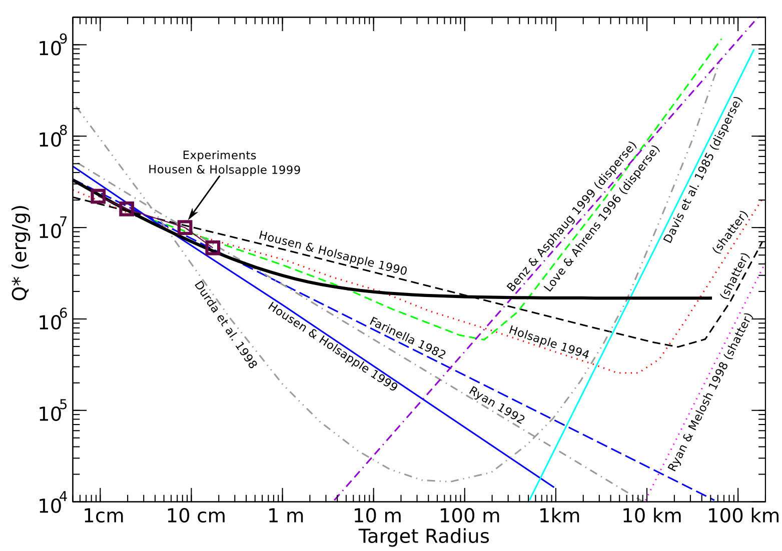

Fig. 7: Disruption model incorporating micro-mechanics-based scaling of strength (bold black line).

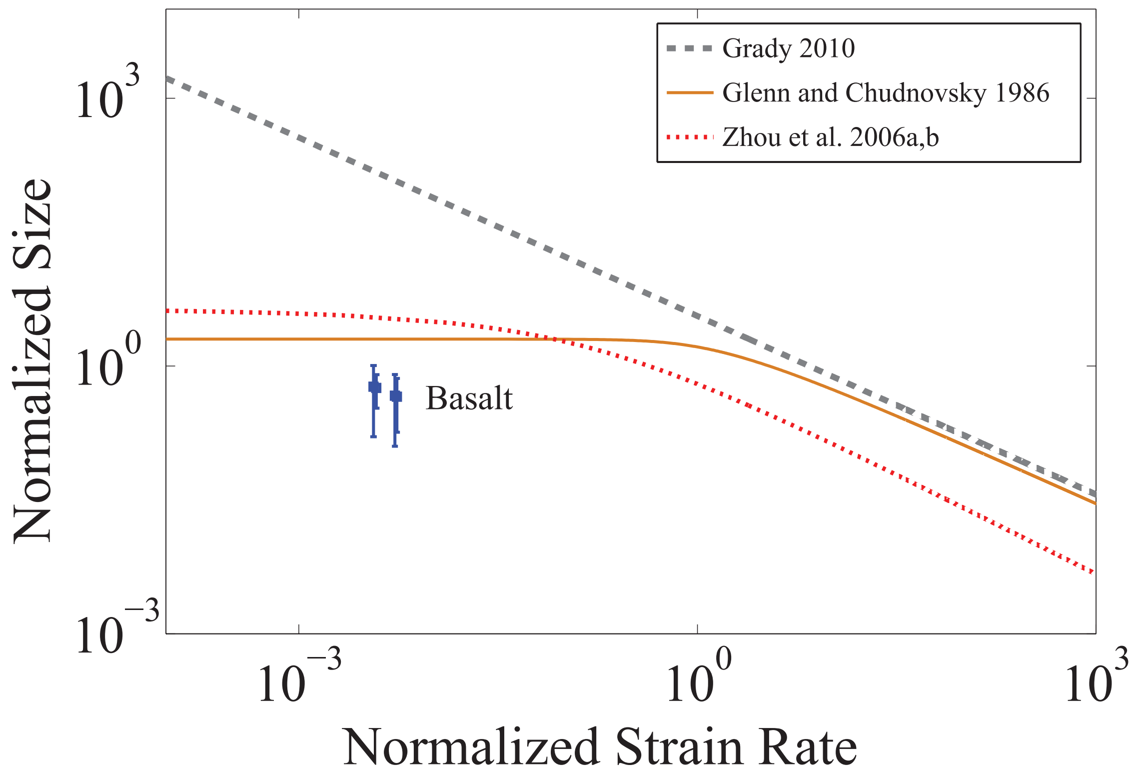

Fig. 8: Experimental fragment size averages of structure-dominated fragmentation compared with the models of Grady (2009b), Glenn and Chudnovsky (1986), Zhou et al. (2006b).

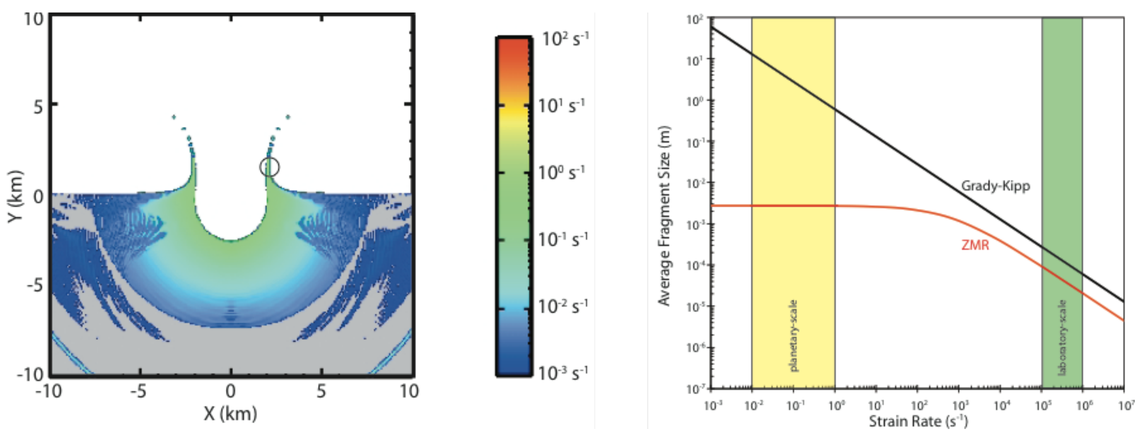

Fig. 9: A. Computed strain rate domains from the impact of a 1km quartz body at 5km/s into a quartz half-space (Ernst et al., 2009). B. Comparison of two different fragmentation models over the computed strain rate domain and the typical laboratory strain rate domain. The ZMR model predicts a much larger amount of fines as a consequence of the impact.